AGU PUBLICATIONS

Geophysical Research Letters

RESEARCH LETTER
10.1002/2014GL062776

Key Points:
- Transient isolated gravity wave generated in situ an NLC layer
- The wave had a tropospheric source due to the passage of an occluded front
- The wave was generated due to strong horizontal wind shears at 5 km altitude

Correspondence to:
P. Dalin,
pdalin@irf.se

Citation:
Dalin, P., et al. (2015), Evidence of the formation of noctilucent clouds due to propagation of an isolated gravity wave caused by a tropospheric occluded front, *Geophys. Res. Lett.*, *42*, 2037–2046, doi:10.1002/2014GL062776.

Received 12 JAN 2015
Accepted 26 FEB 2015
Accepted article online 28 FEB 2015
Published online 25 MAR 2015

Evidence of the formation of noctilucent clouds due to propagation of an isolated gravity wave caused by a tropospheric occluded front

P. Dalin[1,2], A. Pogoreltsev[3], N. Pertsev[4], V. Perminov[4], N. Shevchuk[5], A. Dubietis[6], M. Zalcik[7], S. Kulikov[8], A. Zadorozhny[9], D. Kudabayeva[4,10], A. Solodovnik[11], G. Salakhutdinov[12], and I. Grigoryeva[12]

[1]Swedish Institute of Space Physics, Kiruna, Sweden, [2]Space Research Institute, RAS, Moscow, Russia, [3]Meteorological Forecasts Department, Russian State Hydrometeorological University, St. Petersburg, Russia, [4]A. M. Obukhov Institute of Atmospheric Physics, RAS, Moscow, Russia, [5]Atmospheric Physics Department, Saint Petersburg State University, St. Petersburg, Russia, [6]Department of Quantum Electronics, Vilnius University, Vilnius, Lithuania, [7]NLC CAN AM Network, Edmonton, Alberta, Canada, [8]National Research Centre (NRC "Kurchatov Institute"), Moscow, Russia, [9]Division for Atmospheric Research, Novosibirsk State University, Novosibirsk, Russia, [10]Military Institute of National Guard of Republic of Kazakhstan, Petropavlovsk, Republic of Kazakhstan, [11]Physics Department, North Kazakhstan State University of Manash Kozybayev, Petropavlovsk, Republic of Kazakhstan, [12]National Research Nuclear University "MEPhI" (Moscow Engineering Physics Institute), Moscow, Russia

Abstract We consider a unique case of a propagating internal gravity wave that has generated in situ a compact and thin layer of noctilucent clouds (NLC) at 82.7–85.2 km with a characteristic horizontal scale of 65–70 km, as observed in the Moscow region on the night of 18–19 July 2013. This particular transient isolated gravity wave together with the whole NLC layer suddenly appeared in the clear twilight sky and lasted about 1 h traveling eastward, which differs significantly from previously observed cases of gravity waves propagating through preexisting NLC layers. Our model studies demonstrate that the wave had a tropospheric source connected to the passage of an occluded front. The wave was likely generated due to strong horizontal wind shears at about 5 km altitude.

1. Introduction

Noctilucent clouds (NLC) or night shining clouds are the highest clouds in the Earth's atmosphere, formed in summertime at the mesopause region at 80–90 km. NLC are composed of water ice particles of several tens of nanometer in radius, which effectively scatter sunlight and are readily seen against the twilight sky from the end of May until September from the ground [*Gadsden and Schröder*, 1989]. NLC observed from space are called Polar Mesospheric Clouds (PMC).

NLC are a wonderful natural laboratory for studies of the wave dynamics in a broad spectrum, from small-scale gravity waves (less than 10 km) and turbulent structures [*Fritts et al.*, 1993; *Dalin et al.*, 2010], via medium- and large-scale gravity waves of 10–1000 km [*Witt*, 1962; *Rapp et al.*, 2002] to planetary waves and solar tides [*Kirkwood and Stebel*, 2003; *Dalin et al.*, 2011; *Fiedler et al.*, 2011]. Sometimes, rare and exotic wave phenomena are observed in NLC, such as mesospheric fronts [*Dubietis et al.*, 2011; *Dalin et al.*, 2013] and voids [*Thurairajah et al.*, 2013].

Gravity waves in NLC have been extensively studied in recent decades. Statistical studies have shown that PMC fields contain a broad spectrum of gravity waves with horizontal wavelengths ranging from at least 15 to 400 km [*Chandran et al.*, 2009; *Taylor et al.*, 2011], and that gravity waves exhibit a strong anisotropy in the direction of propagation, with a majority of the waves heading toward the NNE [*Pautet et al.*, 2011]. *Chandran et al.* [2010] have shown that there is a distinct anticorrelation of wave structures with cloud occurrence frequency and correlations with wave-induced temperature perturbations for the latitude range of 70–80°.

The source and generation mechanism of gravity waves observed in the summer mesopause are also topics of current extensive investigations. *Hines* [1968] was probably the first who proposed and studied in detail the relationship between the tropospheric source (fronts and jet streams) and a major wave system observed in NLC. *Yue et al.* [2014] have demonstrated that deep convection in the troposphere can be a source of concentric gravity wave patterns in PMC fields. A review on sources and gravity wave generation mechanisms is given by *Plougonven and Zhang* [2014].

In the present paper, we report a case study on a transient isolated gravity wave observed in the summer mesopause of the Northern Hemisphere, which generated a compact NLC field with peculiar propagation dynamics. By the use of model simulations based on reverse ray tracing and analysis of meteorological data, we identify a source of the observed gravity wave to be of tropospheric origin, namely, the passage of an occluded front.

2. Available Data and Measurement Technique

On 18–19 July 2013 between 22:15 and 23:30 UT, detailed observations of a unique NLC display were made with two synchronized automated digital cameras located at Krasnogorsk and Obninsk (both sites are located near Moscow, Russia). The NLC cameras take images of the twilight sky every minute during the night and are units of the network of ground-based NLC cameras, dedicated to continuous monitoring of NLC activity in the Northern Hemisphere [*Dalin et al*., 2008; *Dubietis et al*., 2011]. The separation distance of 91.25 km between the stations allows the use of a triangulation technique for estimation of the NLC height and horizontal characteristic of the isolated wave. The photographic data have been analyzed using new software developed for NLC image processing [*Dubietis et al*., 2011], which is based on precise calibration of an image using at least 15 reference stars homogeneously distributed in the image. As a result, the accuracy of the height estimation of an object increases up to a single pixel size, which corresponds to 100–600 m for the mean NLC height at 83 km, depending on the focal distance of the lens and the elevation angle. The detailed information on the triangulation technique as well as the error analysis is given in Appendix A.

Meteorological images from the advanced very high resolution radiometer (AVHRR) instrument (aboard the MetOp-B satellite) were used to identify a possible tropospheric source of the isolated wave. The analyzed images were obtained by the Dundee Satellite Receiving Station (the UK).

Met Office synoptic weather charts were analyzed to make conclusions on the weather situation at the times considered.

3. Model Studies

To identify a source of the isolated wave, we performed a reverse ray tracing by applying a 3-D numerical model by *Pogoreltsev and Pertsev* [1996]. The model treats the vertical structure of an acoustic-gravity wave propagating through the atmosphere with realistic height profiles of the background wind and temperature as well as taking into account effects of the thermal conductivity and viscosity. Vertical profiles of the background wind are taken between 0 and 60 km from the Modern Era Retrospective-Analysis for Research and Applications (MERRA) model and between 70 and 100 km from the Global Empirical Wind Model (GEWM) [*Portnyagin and Solovjova*, 2000], and wind profiles have been interpolated between 60 and 70 km. Temperature profiles are taken from the NRLMSISE-00 model [*Picone et al*., 2002]. The reverse ray tracing is made by calculating group velocities of the wave with the height step of 1 km. The input data of the model are the horizontal wavelength of the wave, cyclic frequency, power of a possible source, and its vertical extension as well as vertical profiles of the background wind and temperature. The power of a wave source is a free parameter in the model, which multiplies all wave amplitudes. Since the power of a potential wave source is unknown value in the present case, the power parameter is arbitrarily set to unity. As a result, the backward trajectory, propagation time, and vertical structure of the wave are estimated.

The MERRA model was applied to obtain meteorological data (wind and temperature fields) in the space-time domain considered, using the data with temporal resolution of 3 h and spatial resolution of $1.25° \times 1.25°$ [*Rienecker et al*., 2011].

4. Data Analysis and Discussion

A unique NLC field generated in situ by an isolated gravity wave was captured from Krasnogorsk and Obninsk between 22:15 and 23:30 UT on the night of 18–19 July 2013. The following unusual features were attributed to the case studied:

1. NLC field was in situ generated by an isolated gravity wave.
2. There was a clear sky without any signatures on NLC, but suddenly a compact NLC field emerged in the field of view of two cameras.

Figure 1. Synchronous observations of the transient isolated gravity wave as seen from (top) Krasnogorsk and (bottom) Obninsk on 18 July 2013 at 22:52 UT. A and B marks indicate the two analyzed wave crests.

3. The whole NLC field was mostly confined within two gravity wave crests, which was traveling together with NLC visually from the west to east during a short time period of about 1 h.

We emphasize that apparent movement of the NLC field (not a separate gravity wave) from west to east is a rather unusual feature, since usually NLC move from east to west because of prevailing westward winds at the summer mesopause. The eastward propagating gravity wave seems to be very reasonable since it is not absorbed by the westward stratospheric winds and mesospheric jet, as well as the wave was generated in the troposphere by an eastward moving frontal system as will be shown below. Combining all the three features together, the present case is considered to be unique and significantly differs from those previously observed, which, in general, demonstrate several gravity waves propagating through a preexisting NLC layer. We could not find a similar event either published in the literature or in our huge digital archive for the last 10 years.

Figure 1 illustrates a snapshot of synchronous observations of the isolated wave (analyzed wave crests are marked by A and B) as seen from Krasnogorsk and Obninsk on 18 July 2013 at 22:52 UT. The reader is encouraged to look at the time-lapse video of the event, taken from Krasnogorsk, which can be found at ftp://ftp.irf.se/outgoing/pdalin/NLC/NLC_MOVIE/Krasnogorsk_190713/.

Figure 2 shows the evolution of the NLC display generated by the isolated gravity wave. Small-scale billow waves of 8.5–12 km wavelength have appeared inside the NLC field after 22:26 UT, and additional crests were formed inside the NLC field at 22:39 UT (perhaps, due to the second harmonic generation and wave instability). The leading crest started to deteriorate after 22:52 UT. A bit later, the phase front of the trailing

Figure 2. Six progressive images demonstrating the evolution of the NLC display generated by the transient isolated gravity wave taken from Krasnogorsk on 18–19 July 2013.

crest started to disintegrate as well. By 23:30 UT, the wave developed an undefined complex shape, which was significantly different from the original one. We should note that the NLC field could not be advected into the field of view of the cameras from the north by the background wind since there was a clear sky in the west-north-east sector of the twilight sky before the appearance of the wave (as Figures 1 and 2 demonstrate), and there was a good potential possibility of observing any NLC if they were moving from the north or from the north-east by the background wind. Also, we have checked the evolution of the solar depression angle (SDA), which showed the SDA gradually decreasing from 12.9° to 9.6° during the period of the NLC visibility from 22:15 to 23:30 UT. It means that the contrast (the main parameter defining the NLC visibility) was, as expected, gradually decreasing during this time period as well. Thus, we prove that the present NLC display was not due to either the advection by the background wind or due to increasing visibility by appropriate illumination conditions.

The sudden appearance of the NLC layer between the two wave crests might be explained in terms if there were ice particles of "subvisible" range ($<$30 nm) prior to the wave propagation through the volume of the mesopause considered. *Rapp and Thomas* [2006] have demonstrated that a threshold radius of ice particles, significantly contributing to optically active signal, is about 30 nm, and *Thomas* [1991] has shown that scattered light intensity is a strong function of a particle size, varied as R^6. Thus, it is readily possible that the wave propagation induced additional cooling, forcing the particle size to oscillate between the "visible" and subvisible range. The above considerations allow ignoring other two factors linearly affecting the NLC brightness—a thickness of the layer and particle number density.

Table 1. Parameters of the Transient Isolated Gravity Wave Observed in NLC at 22:52 UT on 18 July 2013

Height Range of the Crests (km)	Height Range of the Trough (km)	Horizontal Wavelength (km)	Azimuth of Propagation (Degrees From North)	Observed Horizontal Phase Velocity (m/s)	Observed Period (min)
84.1–85.2	82.7–83.4	65–70	126	28.3	39.2

One can estimate the lifetime of NLC ice particles. The two crests had a very pronounced brightness compared to the foreground twilight sky; in other words, there were no visible NLC just in front of the crests as well as right behind the crests. The width of the wave crests varied in the range from 2.5 to 6 km. The crests moved with the intrinsic phase speed of about 35–40 m/s relative to ambient air. Thus, dividing the width of the crest by its intrinsic phase speed, we arrive at 1–2.5 min taken for ice particles to oscillate around the visibility threshold.

By applying the triangulation technique, we estimated the height of the two wave crests, of the wave trough, and of small-scale billows within, as well as the horizontal parameters of the large isolated wave (observed phase velocity, observed period, and horizontal wavelength); these parameters are summarized in Table 1.

Figure 3a illustrates the projection of the two wave crests, A and B (the blue lines) on the Earth's surface at 22:52 UT. The additional crest, seen in Figure 1 between the A and B crests, is not shown in Figure 3a, because it has a considerable tilt, higher altitude, and is oriented at a large angle relative to the A and B crests. Using a numerical model by *Pogoreltsev and Pertsev* [1996], we traced the motion and identified a possible source of such a prominent isolated gravity wave. The position of the wave crests as obtained by reverse ray tracing is indicated in Figure 3a by the red lines, suggesting the tropospheric origin of the gravity wave, whose source was located in the troposphere close the Finnish border. The uncertainty of the wave position along the phase velocity vector is shown by the black error bar and is due to ±10% variability in the whole background wind profile. The relatively large error in the wave position arises due to the closeness of the wave phase speed to the background wind speed at about 9 km altitude for this particular case (see below). Nevertheless, the critical level for the wave is not reached. When performing the reverse ray tracing, we have also taken into account the transverse advection of the wave to the phase velocity, which is due to the background wind component normal to the phase velocity vector; the transverse advection was calculated to be about 56 km, which is small compared to the longitudinal travel distance of 660 km. The uncertainty in the wave position due to ±10% variability in the whole temperature profile is small (about 37 km) and is not shown in Figure 3a.

The travel time and horizontal distance along the wave propagation of the model-simulated reverse ray tracing are shown in Figure 3b, the amplitude and phase of horizontal wind perturbations are illustrated in Figure 3c, and the background wind and temperature profiles as functions of height are demonstrated in Figure 3d. The final travel time is 6 h 37 min and final horizontal travel distance is 662 km from the mesopause to an altitude of 5 km. The wave amplitude constantly increases and phase gradually rotates, both without any sharp changes or abrupt rotations, confirming the absence of either any critical level or attenuation. Thus, the gravity wave is assumed to propagate from the troposphere into the mesopause region in the space-time domain considered.

Internal gravity waves (IGWs) in the atmosphere could appear due to nonlinear interactions of mesometeorological and turbulent fields. *Medvedev and Gavrilov* [1995] obtained a mathematical expression of the main component of the nonlinear wave source G_0 (see their equation (18)), which depends on horizontal gradients of the background horizontal velocity components and is determined by the following equation:

$$G_0 = \left(\frac{\partial U}{\partial x}\right)^2 + \frac{\partial U}{\partial y}\frac{\partial V}{\partial x} + \left(\frac{\partial V}{\partial y}\right)^2 \quad (1)$$

where U and V are the zonal and meridional wind components along axes x and y, respectively. In this study, we calculated the wave source G_0 at the 550 hPa pressure level using distributions of background horizontal wind components taken from the MERRA data set at 15:00 UT, which is close to the estimated time of the isolated wave launch at 16:15 UT at 5 km.

Calculated horizontal distribution of the nonlinear wave source G_0 is shown in Figure 4a. Evolution of G_0 field in time and its transport with the mean wind could generate atmospheric IGWs. Green lines show the calculated position of the isolated wave at the launch time and at 5 km according to the wave trajectory shown in Figure 3a. In Figure 4a, one can see that this position is located in the region of the strong positive maximum of $G_0 \sim 3 \cdot 10^{-9}\,\mathrm{s}^{-2}$ situated at 28–32°E and 62–64°N. It is also possible that the advection of the

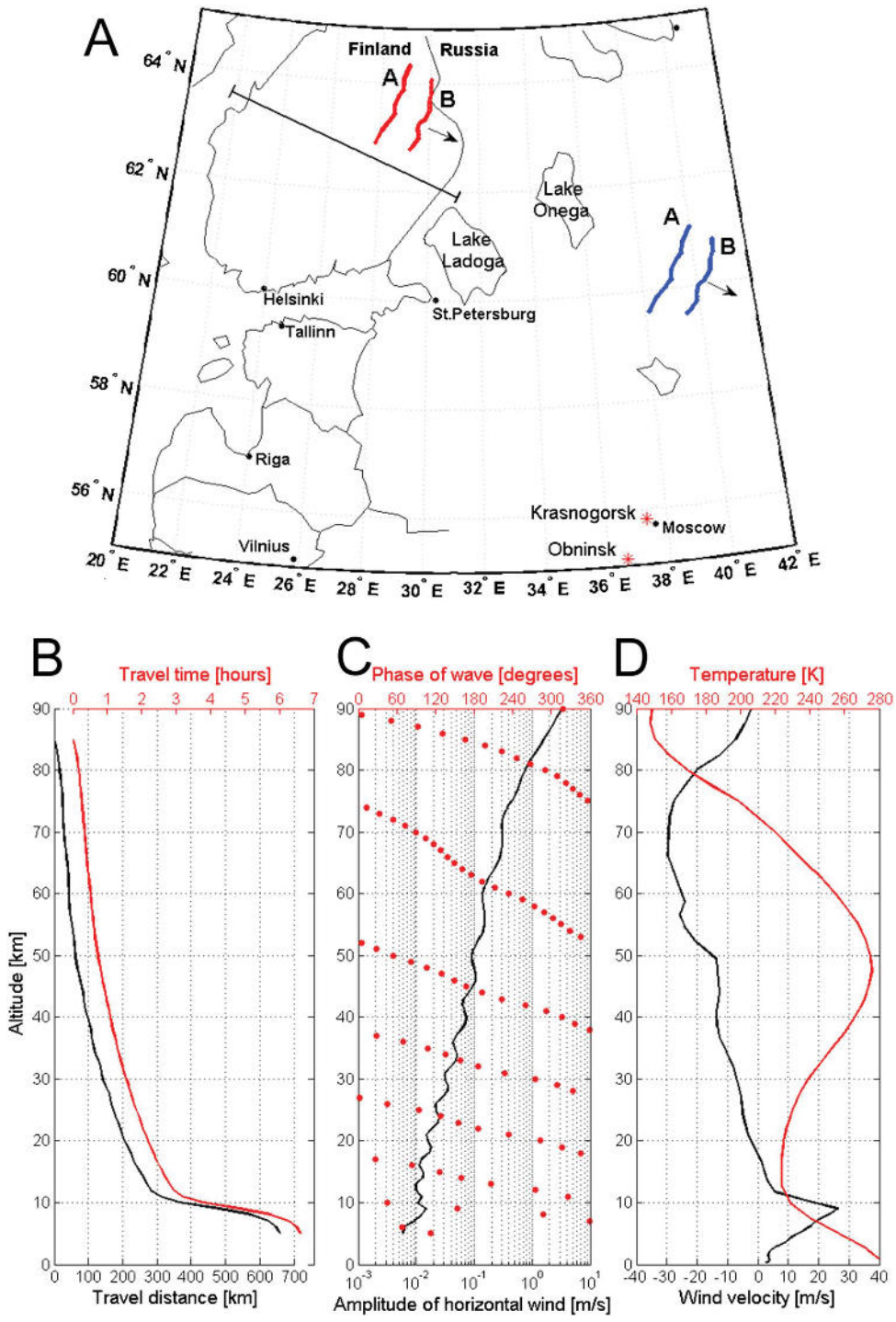

Figure 3. (a) Projection of the two crests of a gravity wave (confining the NLC field) on the Earth's surface. The blue lines are the position of the crests at 84.5 km at 22:52 UT on 18 July 2013; the red lines show the reverse ray trace position at 5 km (6 h 37 min earlier) in accordance to the model simulation. The arrow indicates the direction of the wave motion. A and B marks indicate the position of the projected wave crests shown in Figure 1. The uncertainty of the wave position along the phase velocity vector is shown by the black error bar. (b) The travel time and horizontal distance along the phase velocity vector of the model reverse ray tracing as functions of height. (c) The amplitude of horizontal wind perturbations of the wave and its phase as functions of height. (d) The background wind velocity in the direction of the wave propagation and temperature profile as functions of height. The profiles shown in Figures 3b and 3c were calculated at 15:00 UT on 18 July 2013, with the numerical model by *Pogoreltsev and Pertsev* [1996].

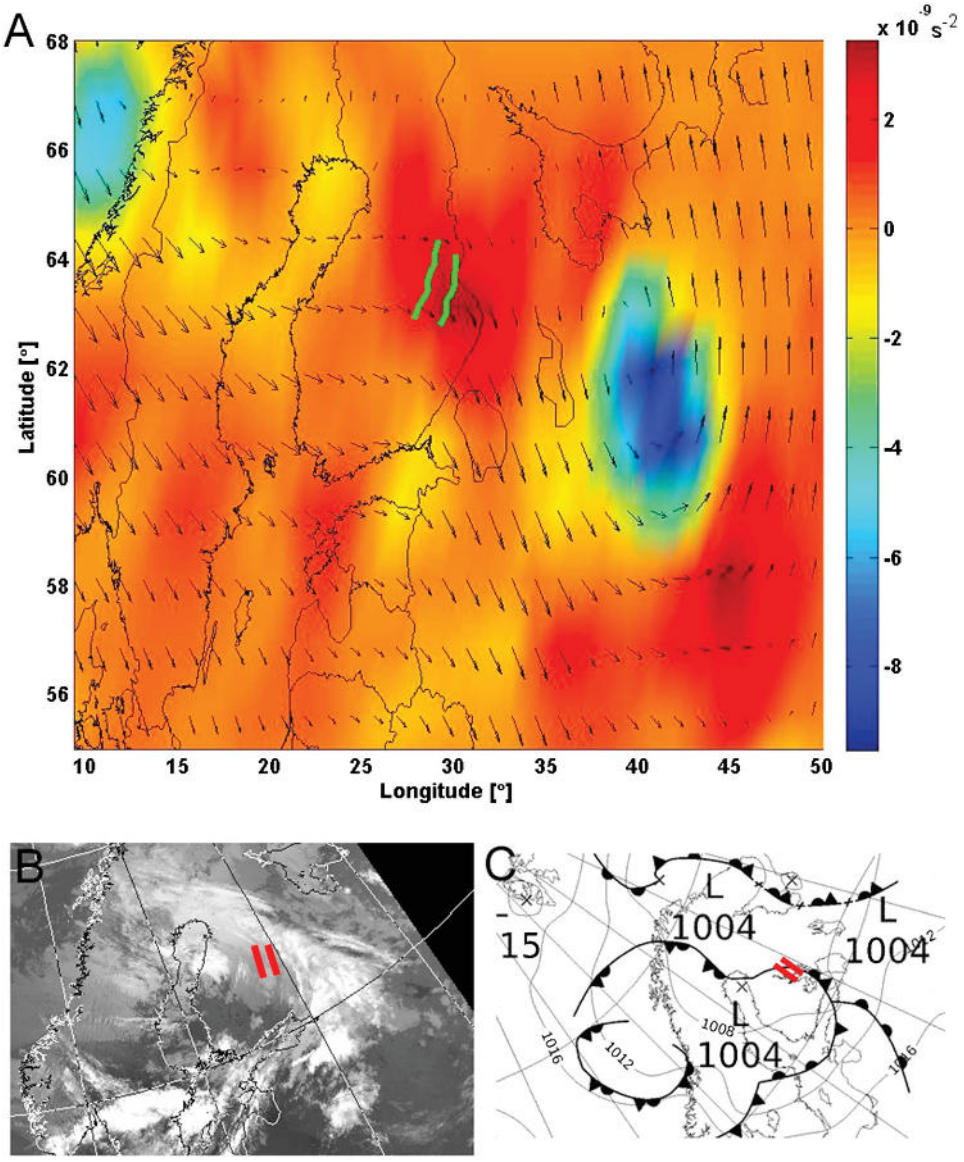

Figure 4. (a) Horizontal distribution of the nonlinear wave source G_0 at 550 hPa at 15:00 UT on 18 July 2013, using equation (18) by *Medvedev and Gavrilov* [1995]. The two green lines represent the estimated positions of the transient isolated gravity wave at 5 km at the launch time. The black arrows indicate the background horizontal wind field. (b) The meteorological image (channel 4, thermal infrared at 10.3–11.3 μm) by the AVHRR/MetOp-B imaging radiometer at 19:19 UT on 18 July 2013. The two red lines indicate the calculated position of the wave crests at the launch time at 16:15 UT at 5 km. The image is kindly provided by the Dundee Satellite Receiving Station (the UK). (c) The synoptic weather chart at 18:00 UT on 18 July 2013. The analysis charts are kindly provided by the Met Office of the UK.

G_0 by the mean wind contributes to the wave generation. Therefore, Figure 4a identifies the presence of the possible activity of gravity wave sources in the troposphere near the trajectory of the isolated wave observed in NLC.

Now it is appropriate to provide an overview of the weather situation in the troposphere using meteorological data analysis and measurements. We found satellite images of the AVHRR/MetOp-B imaging radiometer, which covered the area of interest. Figure 4b shows the AVHRR image at 19:19 UT on 18 July 2013 in the far-infrared channel with overlaid position of the two wave crests (red lines) at the estimated launch time as calculated from the reverse ray tracing. The extended cloud frontal system rotating counterclockwise (cyclonic rotation) is clearly seen in the vicinity of the wave. Since the cyclone represents a rotating pattern,

some filaments of the cloud system are parallel to the orientation of the wave; others are not. It means that some of tropospheric cloud filaments had orientation similar to that of the isolated gravity wave in NLC, which could be readily launched in the direction observed. Figure 4c illustrates synoptic weather charts at 18:00 UT on 18 July 2013. The red lines indicate the projected wave at the time of the launch. Figure 4c confirms the presence of two low-pressure systems in vicinity of the wave generation. A cold front associated with the cyclone is known to produce thunderstorms and heavy showers with gusty winds [*Ahrens*, 1994]. Moreover, the front approaching from the west is an occluded front (marked by alternating cold front triangles and warm front half circles), with the point of occlusion (so called the triple point), which is characterized by most severe weather conditions where the greatest temperature difference occurs. The generation of the wave crests was rather close to the point of occlusion, thus strongly confirming a wave source located in the troposphere and associated with the passage of the occluded front. This is very much in line with *Hines* [1968], who has found a tropospheric source of a major gravity wave observed in NLC, situated in front of the occluded frontal system. It is possible that the shear instability mechanism was involved into the excitation of the gravity wave considered. Very intense shear layers are known to occur near the surface and at upper levels in the course of frontogenesis, leading to shear instability [*Snyder*, 1995; *Plougonven and Zhang*, 2014]. It is confirmed by the result shown in Figure 4a demonstrating strong horizontal wind shears and in turn large values of the wave source G_0 at the position of the wave generation.

5. Conclusions

We have presented a unique case of a propagating internal gravity wave generating in situ a visible NLC layer observed in the Moscow region on the night of 18–19 July 2013. The transient isolated gravity wave formed a compact (65–70 km) and thin layer of NLC at the 82.7–85.2 km level exhibiting peculiar propagation dynamics. Our model studies revealed that this particular isolated wave was generated by a tropospheric source and the wave propagated through the lower and middle atmosphere without attenuation of amplitude. The analysis of meteorological data identified that a source of the prominent and isolated gravity wave could be associated with the passage of an occluded front and/or the point of occlusion. The mechanism of the wave generation was likely due to strong horizontal wind shears at about 5 km altitude.

Appendix A

We follow the main concept of the triangulation technique developed by *Burov* [1959]. The basic equation for the NLC height estimation is as follows:

$$H_1 = \frac{R\cos(E_1)}{\cos(E_1 + S_1)} - R \tag{A1}$$

where

$$\sin(S_1) = \frac{\sin(S)\sin(\psi_2)}{\sin(\lambda)} \tag{A2}$$

where

$$\cos(\lambda) = -\cos(\psi_1)\cos(\psi_2) + \sin(\psi_1)\sin(\psi_2)\cos(S) \tag{A3}$$

where

$$\psi_1 = A_1 - A_{\mathrm{nlc1}} \tag{A4}$$

$$\psi_2 = A_2 - A_{\mathrm{nlc2}} \tag{A5}$$

where R is the mean radius of the curvature on the ellipsoid for point close to the position of NLC; E_1 is the elevation angle of the measured NLC point from the position 1 on the Earth; A_1 and A_2 are the azimuth angles of the base line (the geodetic line between two stations); A_{nlc1} and A_{nlc2} are the measured azimuth angles of the NLC point from the positions 1 and 2; S_1 is the horizontal projection (length) from the position 1 to the measured NLC point projected on the Earth's surface; and S is the angular distance between the stations 1 and 2 on the Earth's surface.

Equation (A1) for the height determination can be considered as a function of two independently measured variables: the elevation angle, E, and azimuth angle, A, of the measured NLC point:

$$F = f(E, A) \tag{A6}$$

According to the theory of error analysis, the mean error in the F is determined by the following equation:

$$m_F = \pm\sqrt{(\partial F/\partial E)^2 m_E{}^2 + (\partial F/\partial A)^2 m_A{}^2} \tag{A7}$$

where m_E and m_A are the errors in elevation and azimuth angles, corresponding to a pixel size. Then after mathematical transformations, we arrive at the following equations for the function partial derivatives:

$$\partial F/\partial E = R \cdot \left(\frac{-\cos(E_1 + S_1)\sin(E_1) + \cos(E_1)\sin(E_1 + S_1)}{\cos^2(E_1 + S_1)}\right) \tag{A8}$$

$$\partial F/\partial A = D_1 \cdot D_2 \cdot D_3 \cdot D_4 \cdot D_5 \cdot D_6 \tag{A9}$$

where

$$D_1 = \frac{R \cdot \cos(E_1) \cdot \sin(E_1 + S_1)}{\cos^2(E_1 + S_1)} \tag{A10}$$

$$D_2 = \left[\sqrt{1 - \left(\frac{\sin(S)\sin(\psi_2)}{\sin(\lambda)}\right)^2}\right]^{-1} \tag{A11}$$

$$D_3 = \cos(\lambda) \tag{A12}$$

$$D_4 = -\left[\sqrt{1 - (\sin(\psi_1)\sin(\psi_2)\cos(S) - \cos(\psi_1)\cos(\psi_2))^2}\right]^{-1} \tag{A13}$$

$$D_5 = \cos(\psi_1)\sin(\psi_2) + \sin(\psi_1)\cos(\psi_2)\cos(S) \tag{A14}$$

In general, the error in the NLC height estimation is dependent on the elevation angle of NLC since the pixel size images different areas of the mesopause at different slant distances. For example, for an NLC elevation angle of 15°, the errors in the terms $\partial F/\partial E$ and $\partial F/\partial A$ are 320.3 km rad^{-1} and 1201.1 km rad^{-1}, respectively. The mean errors in elevation and azimuth angles are 1.061′ and 1.094′, respectively. After substituting the appropriate values into equation (A7), we arrive at the following relation:

$$m_F = \pm\sqrt{0.099^2 + 0.382^2} = \pm 0.395 \text{ km} \tag{A15}$$

We find good agreement between the error estimation given by *Burov* [1959] and our error analysis for the height estimation of NLC.

Acknowledgments
The work was partly supported by the Russian Scientific Foundation under contract 14-17-00685. The authors thank the UK's National Weather Service (the Met Office) for providing the meteorological charts and the Dundee Satellite Receiving Station for providing the meteorological image (channel 4) obtained with the AVHRR/MetOp-B instrument. The authors thank Alister Ling for very useful comments during the manuscript preparation. The paper benefited from constructive comments and suggestions of two anonymous reviewers and of the Editor Paul Williams.

The Editor thanks two anonymous reviewers for their assistance in evaluating this paper.

References

Ahrens, C. D. (1994), *Meteorology Today: An Introduction to Weather, Climate, and the Environment*, West Company, New York.

Burov, M. I. (1959), The photogrammetric method for the height determination of noctilucent clouds, Proceedings of the Conference "Noctilucent Clouds", *Tartu*, 92–111.

Chandran, A., D. W. Rusch, S. E. Palo, G. E. Thomas, and M. J. Taylor (2009), Gravity wave observations in the summertime polar mesosphere from the Cloud Imaging and Particle Size (CIPS) experiment on the AIM spacecraft, *J. Atmos. Sol. Terr. Phys.*, *71*, 392–400, doi:10.1016/j.jastp.2008.09.041.

Chandran, A., D. W. Rusch, A. W. Merkel, S. E. Palo, G. E. Thomas, M. J. Taylor, S. M. Bailey, and J. M. Russell III (2010), Polar mesospheric cloud structures observed from the cloud imaging and particle size experiment on the Aeronomy of Ice in the Mesosphere spacecraft: Atmospheric gravity waves as drivers for longitudinal variability in polar mesospheric cloud occurrence, *J. Geophys. Res.*, *115*, D13102, doi:10.1029/2009JD013185.

Dalin, P., et al. (2008), Ground-based observations of noctilucent clouds with a Northern Hemisphere network of automatic digital cameras, *J. Atmos. Sol. Terr. Phys.*, *70*, 1460–1472, doi:10.1016/j.jastp.2008.04.018.

Dalin, P., N. Pertsev, S. Frandsen, O. Hansen, H. Andersen, A. Dubietis, and R. Balciunas (2010), A case study of the evolution of a Kelvin-Helmholtz wave and turbulence in noctilucent clouds, *J. Atmos. Sol. Terr. Phys.*, *72*(14–15), 1129–1138, doi:10.1016/j.jastp.2010.06.011.

Dalin, P., et al. (2011), A comparison between ground-based observations of noctilucent clouds and Aura satellite data, *J. Atmos. Sol. Terr. Phys.*, *73*(14–15), 2097–2109, doi:10.1016/j.jastp.2011.01.020.

Dalin, P., et al. (2013), First common volume ground-based and space measurements of the mesospheric front in noctilucent clouds, *Geophys. Res. Lett.*, *40*, 6399–6404, doi:10.1002/2013GL058553.

Dubietis, A., et al. (2011), Noctilucent clouds: Modern ground-based photographic observations by a digital camera network, *Appl. Opt.*, *50*(28), F72–F79, doi:10.1364/AO.50.000F72.

Fiedler, J., G. Baumgarten, U. Berger, P. Hoffmann, N. Kaifler, and F.-J. Lübken (2011), NLC and the background atmosphere above ALOMAR, *Atmos. Chem. Phys.*, *11*, 5701–5717, doi:10.5194/acp-11-5701-2011.

Fritts, D. C., J. R. Isler, G. E. Thomas, and Ø. Andreassen (1993), Wave breaking signatures in noctilucent clouds, *Geophys. Res. Lett.*, *20*(19), 2039–2042, doi:10.1029/93GL01982.

Gadsden, M., and W. Schröder (1989), *Noctilucent Clouds*, Springer, New York.

Hines, C. O. (1968), A possible source of waves in noctilucent clouds, *J. Atmos. Sci.*, *25*, 937–942.

Kirkwood, S., and K. Stebel (2003), Influence of planetary waves on noctilucent clouds occurrence over NW Europe, *J. Geophys. Res.*, *108*(D8), 8440, doi:10.1029/2002JD002356.

Medvedev, A. S., and N. M. Gavrilov (1995), The nonlinear mechanism of gravity wave generation by meteorological motions in the atmosphere, *J. Atmos. Sol. Terr. Phys.*, *57*(11), 1221–1231.

Pautet, P.-D., J. Stegman, C. M. Wrasse, K. Nielsen, H. Takahashi, M. J. Taylor, K. W. Hoppel, and S. D. Eckermann (2011), Analysis of gravity waves structures visible in noctilucent cloud images, *J. Atmos. Sol. Terr. Phys.*, *73*(14–15), 2082–2090, doi:10.1016/j.jastp.2010.06.001.

Picone, J. M., A. E. Hedin, D. P. Drob, and A. C. Aikin (2002), NRLMSISE-00 empirical model of the atmosphere: Statistical comparisons and scientific issues, *J. Geophys. Res.*, *107*(A12), 1468, doi:10.1029/2002JA009430.

Plougonven, R., and F. Zhang (2014), Internal gravity waves from atmospheric jets and fronts, *Rev. Geophys.*, *52*, 33–76, doi:10.1002/2012RG000419.

Pogoreltsev, A. I., and N. N. Pertsev (1996), The influence of background wind on the formation of the acoustic-gravity wave structure in the thermosphere, *Atmos. Oceanic Phys.*, *31*(6), 723–731.

Portnyagin, Y. I., and T. V. Solovjova (2000), Global empirical wind model for the upper mesosphere/lower thermosphere. I. Prevailing wind, *Ann. Geophys.*, *18*, 300–315.

Rapp, M., and G. E. Thomas (2006), Modeling the microphysics of mesospheric ice particles: Assessment of current capabilities and basic sensitivities, *J. Atmos. Sol. Terr. Phys.*, *68*, 715–744.

Rapp, M., F.-J. Lübken, A. Müllemann, G. Thomas, and E. Jensen (2002), Small scale temperature variations in the vicinity of NLC: Experimental and model results, *J. Geophys. Res.*, *107*(D19), 4392, doi:10.1029/2001JD001241.

Rienecker, M. M., et al. (2011), MERRA: NASA's Modern-Era Retrospective Analysis for Research and Applications, *J. Clim.*, *24*, 3624–3648, doi:10.1175/JCLI-D-11-00015.1.

Snyder, C. (1995), Stability of steady fronts with uniform potential vorticity, *J. Atmos. Sci.*, *52*(6), 724–736.

Taylor, M. J., P.-D. Pautet, Y. Zhao, C. E. Randall, J. Lumpe, S. M. Bailey, J. Carstens, K. Nielsen, J. M. Russell III, and J. Stegman (2011), High-latitude gravity wave measurements in noctilucent clouds and polar mesospheric clouds, in *Aeronomy of the Earth's Atmosphere and Ionosphere*, *IAGA Spec. Sopron Book Ser.*, vol. 2, edited by B. Hulqvist, pp. 93–105, Springer, New York.

Thomas, G. E. (1991), Mesospheric clouds and physics of the mesosphere region, *Rev. Geophys.*, *29*(4), 553–575, doi:10.1029/91RG01604.

Thurairajah, B., S. M. Bailey, D. E. Siskind, C. E. Randall, M. J. Taylor, and J. M. Russell III (2013), Case study of an ice void structure in polar mesospheric clouds, *J. Atmos. Sol. Terr. Phys.*, *104*, 224–233, doi:10.1016/j.jastp.2013.02.001.

Witt, G. (1962), Height, structure and displacements of noctilucent clouds, *Tellus*, *14*, 1–18.

Yue, J., B. Thurairajah, L. Hoffmann, J. Alexander, A. Chandran, M. J. Taylor, J. M. Russell III, C. E. Randall, and S. M. Bailey (2014), Concentric gravity waves in polar mesospheric clouds from the Cloud Imaging and Particle Size experiment, *J. Geophys. Res. Atmos.*, *119*, 5115–5127, doi:10.1002/2013JD021385.